PHYSICS OF FLUIDS **27**, 012101 (2015)

# Stability results for multi-layer radial Hele-Shaw and porous media flows

Craig Gin and Prabir Daripa[a)]
*Department of Mathematics, Texas A&M University, College Station, Texas 77843, USA*

(Received 26 August 2014; accepted 11 December 2014; published online 6 January 2015)

Motivated by stability problems arising in the context of chemical enhanced oil recovery, we perform linear stability analysis of Hele-Shaw and porous media flows in radial geometry involving an arbitrary number of immiscible fluids. Key stability results obtained and their relevance to the stabilization of fingering instability are discussed. Some of the key results, among many others, are (i) absolute upper bounds on the growth rate in terms of the problem data; (ii) validation of these upper bound results against exact computation for the case of three-layer flows; (iii) stability enhancing injection policies; (iv) asymptotic limits that reduce these radial flow results to similar results for rectilinear flows; and (v) the stabilizing effect of curvature of the interfaces. Multi-layer radial flows have been found to have the following additional distinguishing features in comparison to rectilinear flows: (i) very long waves, some of which can be physically meaningful, are stable; and (ii) eigenvalues can be complex for some waves depending on the problem data, implying that the dispersion curves for one or more waves can contact each other. Similar to the rectilinear case, these results can be useful in providing insight into the interfacial instability transfer mechanism as the problem data are varied. Moreover, these can be useful in devising smart injection policies as well as controlling the complexity of the long-term dynamics when drops of various immiscible fluids intersperse among each other. As an application of the upper bound results, we provide stabilization criteria and design an almost stable multi-layer system by adding many layers of fluid with small positive jumps in viscosity in the direction of the basic flow.  [http://dx.doi.org/10.1063/1.4904983]

## I. INTRODUCTION

There have been numerous studies on rectilinear and radial displacements of immiscible fluids in a Hele-Shaw (HS) cell (see review articles[1,2]). The relation between the velocity and pressure gradient in a Hele-Shaw cell for each phase is well known to be Darcy's law, the same equation that holds for fluid flow in porous media with an equivalent permeability. Because of this analogy and accessibility of the Hele-Shaw cell setup in the laboratory, viscous fingering instability in a Hele-Shaw cell has been studied experimentally, analytically, and numerically for over half a century in order to get insight into the phenomenon of viscous fingering in porous media.

The viscous fingering instability occurs when a viscous fluid is displaced by another one of lower viscosity in the confined geometry of a HS cell.[3] This mechanism is widely viewed as a paradigm for interfacial pattern formation in various physical systems. Instabilities at the moving interface evolve and eventually form a variety of complex interfacial patterns through repeated tip splitting. This problem is generic for many fields, including chemical enhanced oil recovery (EOR), cell fragmentation, growth of tumors, mixing in multi-phase flow, crystal growth, and flow in granular media. In the case of radial HS flow, the curvature of the interface acts as a source term which further accentuates the tip splitting, forming more complex patterns. Over the past two

a)Author to whom correspondence should be addressed. Electronic mail: daripa@math.tamu.edu

 

decades, there have been many studies of radial Hele-Shaw flows in order to get important insight into the onset and development of pattern forming processes. Some of these studies were carried out with the goal of controlling and minimizing viscous fingering by various means including time-dependent injection rates and the use of a non-Newtonian injection fluid. In this paper, we will discuss another way to control viscous fingering by injecting a sequence of fluids whose stability is the subject of this paper.

Radial fingering involving immiscible fluids in a Hele-Shaw cell was first experimentally and theoretically studied by Paterson.[4] Many studies have been performed since then on radial displacement,[5–10] but almost all involve two layers of fluids separated by one interface initially. Later Cardoso and Woods[11] studied linear stability of three-layer radial immiscible displacement and studied formation of drops due to break up of the thin annular region. They studied the case where the mobilities of three fluids were such that the inner interface is stable and the outer interface is unstable. This way the thin annular region will break into droplets due to the growth of disturbances on the outer interface. To date, there has not been any study of the multi-layer radial displacement which we address in this paper.

Motivation for the study presented in this paper comes from many injection policies that are in practice for EOR even though the study has much wider applicability and relevance. It is not so uncommon to flood oil reservoirs with a sequence of different simple and complex fluids during enhanced oil recovery in order to maximize productivity.[12–22] One of the objectives behind such practices in the context of EOR is to minimize fingering instability (viscous fingering). Such a flooding process involves more than one interface depending on the number of injected immiscible fluids. To effectively make use of such flooding strategies, it is necessary to understand the viscous fingering mechanism in such a multi-layer setting. A first step in this direction is to perform linear stability analysis of multi-layer porous media flows. Currently, there is not much theoretical work in this direction except for a few recent works[23–25] in rectilinear geometry. In this paper, we consider multi-layer **radial** flows in a Hele-Shaw cell which is a simple model of flows around injection and production wells in porous media. In particular, we perform linear stability analysis involving an arbitrary number of fluid layers to obtain dispersion relations and upper bounds on the growth rate which are then used to design more stable injection schemes. The results of this study are shown to reduce to the results for rectilinear flows in appropriate limits.

Even though we study this problem in the EOR context, this study is relevant for many other natural and industrial situations where multi-layer flows arise. For example, during volcanic eruptions magmas of various compositions and viscosities rise from the depth of fissures in the Earth's crust which can be viewed as multi-layered flows with mixing occurring between magmas of different viscosities due to hydrodynamic instabilities. As stated in Cardoso and Woods,[11] the extent of mixing occurring during such ascent has a key role in controlling the composition of the magma, which is an issue of central importance in petrology.[26] There are many situations where instabilities are desired as in drop formation through break up of various layers and in enhanced mixing between miscible phases. In all these, an understanding of linear instability provides an insight into the possible control mechanisms of viscous fingering, either to enhance it or suppress it.

The paper is laid out as follows. In Sec. II, we formulate the linear stability problem for two-layer **radial** flows because the linearized stability equations, including the ones at the interface, will be the building block for setting up the stability problem for multi-layer radial flows in Sec. III. In Sec. III A, we first develop the eigenvalue problem for 3-layer **radial** flows from linear stability analysis and then analyze this problem for the dispersion relation and upper bounds on the growth rate. The treatment in this section becomes the building block for the stability analysis of the multi-layer case with an arbitrary number of layers which is presented in Sec. III B. In Sec. III B, we derive upper bounds on the growth rate for multi-layer **radial** flows. Section III C discusses some special cases. In particular, we show how the previously obtained result on the upper bound on the growth rate for the rectilinear geometry (see Ref. 23) can be recovered from the results obtained in this paper for the multi-layer radial geometry. In Sec. IV, we show using the upper bounds on the growth rate for multi-layer radial flows that an otherwise unstable two-layer radial flow can be significantly stabilized by the addition of many layers of fluid with small positive jumps in viscosity. Numerical results are presented in Sec. V. Finally, we conclude in Sec. VI.

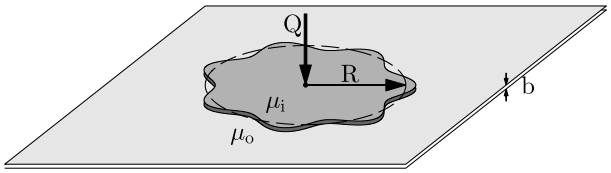


FIG. 1. Radial flow in a Hele-Shaw cell.

## II. PRELIMINARIES

We start by deriving the equations for two-layer Hele-Shaw flows. Although this is done in numerous other works[4,7,11] with the use of the potential function, we follow an approach that does not use the potential function. That is because our approach can be easily adapted to study flows with variable viscosity fluids which do not have a potential function. This is of considerable interest to EOR and will be the subject of a sequel to this paper.

We consider a Hele-Shaw flow in which two incompressible, immiscible fluids are present. The less viscous fluid is injected into the center of the cell, displacing the more viscous fluid. We denote the viscosity of the less viscous inner fluid by $\mu_i$ and the viscosity of the more viscous outer fluid by $\mu_o$ (Figure 1).

By averaging across the gap, we may consider a two-dimensional flow domain in polar coordinates, $\Omega := (r,\theta) = \mathbb{R}^2$. The fluid flow is governed by the following equations:

$$\nabla \cdot \mathbf{u} = 0, \quad \nabla\, p = -\mu\, \mathbf{u}. \tag{1}$$

The first equation $(1)_1$ is the continuity equation for incompressible flow, and the second equation $(1)_2$ is Darcy's law.[27] We start with the fluids separated by a circular interface with radius $R_0$. Fluid is then injected into the cell at the origin at a constant injection rate, $Q$. This set-up is shown in Figure 2.

The equations admit a simple basic solution in which all of the fluid moves outward radially with velocity $\mathbf{u}^b := \left(u_r^b, u_\theta^b\right) = (Q/2\pi r, 0)$. The interface remains circular and its radius is given by $R(t) = \sqrt{Qt/\pi + R_0^2}$. The pressure, $p_b = p_b(r)$, may be obtained by integrating equation $(1)_2$. We perturb the basic solution $\left(u_r^b, u_\theta^b, p_b\right)$ by $(\tilde{u_r}, \tilde{u_\theta}, \tilde{p})$ where the disturbances are assumed to be small. We plug these into equations (1) and only keep terms that are linear with respect to disturbances. Since equations (1) are, in fact, linear, the disturbances satisfy the same equations. Therefore,

$$\frac{\partial \tilde{u_r}}{\partial r} + \frac{\tilde{u_r}}{r} + \frac{1}{r}\frac{\partial \tilde{u_\theta}}{\partial \theta} = 0, \quad \frac{\partial \tilde{p}}{\partial r} = -\mu \tilde{u_r}, \quad \frac{1}{r}\frac{\partial \tilde{p}}{\partial \theta} = -\mu \tilde{u_\theta}. \tag{2}$$

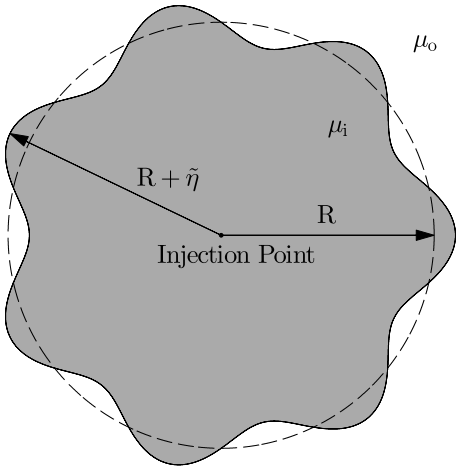


FIG. 2. Two-layer radial Hele-Shaw flow.

We investigate the growth of these disturbances by the method of normal modes. Since the basic solution is time dependent, due to the time dependence of the position of the interface, the growth rate is also time dependent. We consider the following ansatz for the disturbances:

$$(\tilde{u_r}, \tilde{u_\theta}, \tilde{p}) = (f(r), \tau(r), \psi(r)) e^{in\theta + \int_0^t \sigma(s)ds}, \tag{3}$$

where $n$ denotes the wavenumber of the disturbance. Plugging this ansatz into equations $(2)_1$ and $(2)_3$ gives

$$\tau(r) = \frac{i}{n}(f(r) + rf'(r)), \qquad \psi(r) = -\frac{r\mu}{n^2}(f(r) + rf'(r)). \tag{4}$$

We then cross-differentiate the pressure equation, $(2)_2$ and $(2)_3$. Taking $\frac{\partial}{\partial\theta}$ of $(2)_2$ and $\frac{\partial}{\partial r}$ of $(2)_3$ yields

$$\frac{\partial^2 \tilde{p}}{\partial r \partial\theta} = -\mu \frac{\partial \tilde{u_r}}{\partial\theta}, \qquad \frac{\partial^2 \tilde{p}}{\partial\theta \partial r} = \frac{1}{r}\frac{\partial \tilde{p}}{\partial\theta} - r\mu \frac{\partial \tilde{u_\theta}}{\partial r}.$$

Setting these equal gives

$$-\mu \frac{\partial \tilde{u_r}}{\partial\theta} = \frac{1}{r}\frac{\partial \tilde{p}}{\partial\theta} - r\mu \frac{\partial \tilde{u_\theta}}{\partial r}. \tag{5}$$

We use the ansatz (3) in equation (5) and get

$$-i\,\mu\, n f(r) e^{in\theta + \int_0^t \sigma(s)ds} = \frac{in}{r}\psi(r) e^{in\theta + \int_0^t \sigma(s)ds} - r\mu\tau'(r) e^{in\theta + \int_0^t \sigma(s)ds}. \tag{6}$$

Using (4) in (6), we get: $-i\,\mu\, n f(r) = -\mu\frac{i}{n}(f(r) + rf'(r)) - r\mu\frac{i}{n}(2f'(r) + rf''(r))$. With some algebraic manipulation, we get the following ordinary differential equation for $f(r)$:

$$\left(r^3 f'(r)\right)' - \left(n^2 - 1\right) r f(r) = 0. \tag{7}$$

The solution must also satisfy linearized kinematic and dynamic interface conditions. Let $\tilde{\eta}(\theta, t)$ be the disturbance of the interface. Then the position of the interface is given by $\eta(\theta, t) = R(t) + \tilde{\eta}$. The linearized kinematic condition is given by

$$\frac{\partial \tilde{\eta}}{\partial t} = \tilde{u_r}(R) - \tilde{\eta}\frac{Q}{2\pi R^2}, \tag{8}$$

where $\tilde{u_r}$ is continuous at $r = R$. Consistent with the ansatz (3), we assume $\tilde{\eta} = \tilde{\eta}_0\, e^{in\theta + \int_0^t \sigma(s)ds}$ for some constant $\tilde{\eta}_0$. We use this in (8) along with the ansatz $(3)_1$ for $\tilde{u_r}$ and get

$$\tilde{\eta}(\theta, t) = \frac{f(R)}{\sigma + \frac{Q}{2\pi R^2}} e^{in\theta + \int_0^t \sigma(s)ds}. \tag{9}$$

Next, we consider the linearized dynamic interface condition

$$p^+(\eta) - p^-(\eta) = -T\left(\frac{1}{R} - \frac{\tilde{\eta}}{R^2} - \frac{1}{R^2}\frac{\partial^2 \tilde{\eta}}{\partial\theta^2}\right),$$

where $T$ is the interfacial tension and the "+" and "−" superscripts denote the right and left limit values, respectively. The values of the pressure are given within linear approximation by

$$p^+(\eta) = p_b^+(R) + \tilde{p}^+(R) + \tilde{\eta}\frac{\partial p_b^+}{\partial r}(R), \qquad p^-(\eta) = p_b^-(R) + \tilde{p}^-(R) + \tilde{\eta}\frac{\partial p_b^-}{\partial r}(R).$$

The pressure of the basic solution satisfies $p_b^+(R) - p_b^-(R) = -T/R$. Additionally, since the pressure of the basic solution satisfies equation $(1)_2$ with $u_r = Q/(2\pi r)$, we have that $\frac{\partial p_b^+}{\partial r} = -Q\mu^+/(2\pi r)$ and $\frac{\partial p_b^-}{\partial r} = -Q\mu^-/(2\pi r)$. Therefore,

$$\left\{\tilde{p}^+(R) - \tilde{\eta}\frac{Q\mu^+}{2\pi R}\right\} - \left\{\tilde{p}^-(R) - \tilde{\eta}\frac{Q\mu^-}{2\pi R}\right\} = T\frac{\tilde{\eta} + \frac{\partial^2\tilde{\eta}}{\partial\theta^2}}{R^2}. \tag{10}$$

Plugging the ansatz into this interface condition, we get

$$\left\{\psi^+(R) - \frac{f(R)}{\sigma + \frac{Q}{2\pi R^2}}\frac{Q\mu^+}{2\pi R}\right\} - \left\{\psi^-(R) - \frac{f(R)}{\sigma + \frac{Q}{2\pi R^2}}\frac{Q\mu^-}{2\pi R}\right\}$$
$$= \frac{T}{R^2}\left\{\frac{f(R)}{\sigma + \frac{Q}{2\pi R^2}} + \frac{\partial^2}{\partial\theta^2}\left(\frac{f(R)}{\sigma + \frac{Q}{2\pi R^2}}\right)\right\}.$$

Using (4), the equation becomes

$$\left\{-\frac{R\mu^+(R)}{n^2}(f(R) + R(f^+)'(R)) - \frac{f(R)}{\sigma + \frac{Q}{2\pi R^2}}\frac{Q\mu^+}{2\pi R}\right\}$$
$$-\left\{-\frac{R\mu^-(R)}{n^2}(f(R) + R(f^-)'(R)) - \frac{f(R)}{\sigma + \frac{Q}{2\pi R^2}}\frac{Q\mu^-}{2\pi R}\right\} = \frac{T}{R^2}\frac{1-n^2}{\sigma + \frac{Q}{2\pi R^2}}f(R).$$

Multiplying by $\left(\sigma + \frac{Q}{2\pi R^2}\right) Rn^2$ and rearranging gives

$$\left(\sigma + \frac{Q}{2\pi R^2}\right) R^3\{\mu^-(f^-)'(R) - \mu^+(f^+)'(R)\}$$
$$= \left\{\left(\sigma + \frac{Q}{2\pi R^2}\right) R^2(\mu^+ - \mu^-) + \frac{Qn^2}{2\pi}(\mu^+ - \mu^-) - T\frac{n^4 - n^2}{R}\right\} f(R). \tag{11}$$

The eigenvalue problem is given by the equations (7) and (11). Two linearly independent solutions of (7) are $f(r) = r^{n-1}$ and $f(r) = r^{-n-1}$. Since we require that $f(r) \to$ finite as $r \to 0$ and $f(r) \to 0$ as $r \to \infty$, the solution of the eigenvalue problem is given by

$$f(r) = \begin{cases} f(R)\left(\frac{r}{R}\right)^{n-1}, & r < R \\ f(R)\left(\frac{R}{r}\right)^{n+1}, & r > R \end{cases}.$$

By differentiating these equations, we get

$$(f^-)'(r) = \frac{f(R)}{R}(n-1)\left(\frac{r}{R}\right)^{n-2}, \qquad (f^+)'(r) = -\frac{f(R)}{R}(n+1)\left(\frac{R}{r}\right)^{n+2}.$$

We plug these into (11) and use that $\mu^- = \mu_i$ and $\mu^+ = \mu_o$ to get

$$\left(\sigma + \frac{Q}{2\pi R^2}\right) R^3\left\{\mu_i\frac{f(R)}{R}(n-1) + \mu_o\frac{f(R)}{R}(n+1)\right\}$$
$$= \left\{\left(\sigma + \frac{Q}{2\pi R^2}\right) R^2(\mu_o - \mu_i) + \frac{Qn^2}{2\pi}(\mu_o - \mu_i) - T\frac{n^4 - n^2}{R}\right\} f(R).$$

Solving this equation for $\sigma$ gives the classical result for the growth rate of the interfacial disturbance of the two-layer radial Hele-Shaw problem[4]

$$\sigma = \frac{Qn}{2\pi R^2}\frac{\mu_o - \mu_i}{\mu_o + \mu_i} - \frac{Q}{2\pi R^2} - \frac{T}{\mu_o + \mu_i}\frac{n\left(n^2 - 1\right)}{R^3}. \tag{12}$$

Several facts are obvious from this formula: (i) short waves are stable for any non-zero value of $T$ as expected; (ii) very long waves on the circular interface of any radius are stable when $T = 0$; (iii) there are very long waves with wavenumber below a critical value for which the circular interface of very small radius is stable for finite values of $T$. This is due to the high curvature of the interface when the stabilization effect of interfacial tension overcomes the destabilization effect of mobility jump across the interface; These effects (ii) and (iii) are different from that in rectilinear flow; (iv) the most dangerous wavenumber, $n = n_m$, is easily found and is given by $n_m = \sqrt{QR(\mu_o - \mu_i)/(6\pi T) + 1/3}$. The most dangerous wavenumber $n_m$ is a monotonically

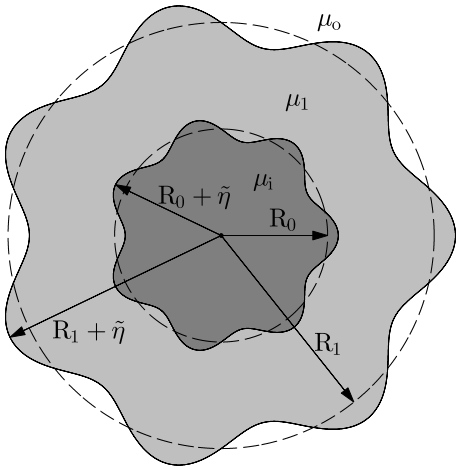


FIG. 3. Three-layer flow.

decreasing function of interfacial tension $T$. The corresponding maximum growth rate, $\sigma_M$, can easily be found from (12) with $n = n_m$.

Finally, (v) there exists an optimal value of $T = T_o$ which minimizes $\sigma_M$. This value is given by $T_o = QR(\mu_o - \mu_i)/4\pi$ and easily follows from taking the derivative of (12) with $n = n_m$ with respect to $T$ and setting it to zero. However, this minimization of $\sigma_M$ is performed over all positive values of $n$. The only physically relevant values of the wavenumber $n$ are positive integers. It can be seen from equation (12) that for any $n > 1$, $\sigma$ decreases monotonically as $T$ increases. It can be checked from the formula for $n_m$ in item (iv) above that $n_m = 1$ when $T = T_o$. Also, $\sigma(n)$ is a decreasing function of $n$ for all $n > n_m$. Therefore, when $T \geq T_o$, $n = 1$ will be the most unstable wave and hence from (12), $\min \sigma_M = -(Q\mu_i)/(\pi R^2(\mu_o + \mu_i))$. This means that the flow is actually stable since $\sigma_M < 0$ when $T > T_o$ regardless of the radius of the circular interface. This leads to a possibly new and important observation. A circular interface of any radius $R$ moving outward at any velocity displacing a fluid of viscosity $\mu_o$ is stable if interfacial tension $T = QR(\mu_o - \mu_i)/4\pi$ where $Q$ is the volumetric injection rate of the displacing fluid having viscosity $\mu_i$.

## III. LINEAR STABILITY ANALYSIS FOR MULTI-LAYER RADIAL FLOWS

### A. Three-layer flows

We now wish to extend the results of Sec. II to flows that contain three layers of fluid (Figure 3). Each fluid region is initially separated from the neighboring fluid regions by a circular interface. The least viscous fluid, with viscosity $\mu_i$, is injected into the Hele-Shaw cell with constant injection rate $Q$. The most viscous fluid, with viscosity $\mu_o$, is the outermost fluid. The intermediate fluid has viscosity $\mu_1$ where $\mu_i < \mu_1 < \mu_o$. The basic solution consists of all fluid moving outward radially with velocity $\mathbf{u}^b = (Q/2\pi r, 0)$. The interfaces remain circular with $R_0$ denoting the radius of the inner interface and $R_1$ denoting the radius of the outer interface. These radii are given by $R_0(t) = \sqrt{Qt/\pi + R_0^2(0)}$ and $R_1(t) = \sqrt{Qt/\pi + R_1^2(0)}$. The pressure is obtained by integrating equation $(1)_2$.

Equation (7) holds within each layer of fluid. Therefore, the solution, $f(r)$, is of the form

$$f(r) = \begin{cases} A_1 r^{n-1} + B_1 r^{-(n+1)}, & r < R_0 \\ A_2 r^{n-1} + B_2 r^{-(n+1)}, & R_0 < r < R_1 \\ A_3 r^{n-1} + B_3 r^{-(n+1)}, & r > R_1 \end{cases} .$$

In order to ensure that the disturbances go to zero as $r \to \infty$ and to avoid a singularity at $r = 0$, we require that $B_1 = 0$ and $A_3 = 0$. Therefore,

$$(f^-)'(R_0) = \frac{(n-1)f(R_0)}{R_0}, \qquad (f^+)'(R_1) = -\frac{(n+1)f(R_1)}{R_1}. \tag{13}$$

Using the interface condition (11) at the inner interface along with $(13)_1$, we get

$$\left(\sigma + \frac{Q}{2\pi R_0^2}\right)\mu_1 R_0^3 (f^+)'(R_0) = -\left[E_0 + \frac{Q\mu_1}{2\pi} - \sigma R_0^2(n\mu_i - \mu_1)\right] f(R_0), \tag{14}$$

where

$$E_0 = \frac{Qn^2}{2\pi}(\mu_1 - \mu_i) - \frac{Qn}{2\pi}\mu_i - T_0\frac{n^4 - n^2}{R_0}, \tag{15}$$

and $T_0$ denotes the interfacial tension at the inner interface. For the outer interface, we use $(13)_2$ to get

$$\left(\sigma + \frac{Q}{2\pi R_1^2}\right)\mu_1 R_1^3 (f^-)'(R_1) = \left[E_1 - \frac{Q\mu_1}{2\pi} - \sigma R_1^2(\mu_1 + n\mu_o)\right] f(R_1), \tag{16}$$

where

$$E_1 = \frac{Qn^2}{2\pi}(\mu_o - \mu_1) - \frac{Qn}{2\pi}\mu_o - T_1\frac{n^4 - n^2}{R_1}, \tag{17}$$

and $T_1$ denotes the interfacial tension at the outer interface.

### 1. Dispersion relation

Recall that the form of $f(r)$ in the region $R_0 < r < R_1$ is $f(r) = A_2 r^{n-1} + B_2 r^{-(n+1)}$. Plugging this form into (14) and simplifying yields

$$\left[E_0 + \frac{Qn}{2\pi}\mu_1 + \sigma R_0^2 n(\mu_1 - \mu_i)\right] R_0^n A_2 + \left[E_0 - \frac{Qn}{2\pi}\mu_1 - \sigma R_0^2 n(\mu_1 + \mu_i)\right] R_0^{-n} B_2 = 0. \tag{18}$$

Likewise, we use (16) to find that

$$\left[E_1 - \frac{Qn}{2\pi}\mu_1 - \sigma R_1^2 n(\mu_o + \mu_1)\right] R_1^n A_2 + \left[E_1 + \frac{Qn}{2\pi}\mu_1 - \sigma R_1^2 n(\mu_o - \mu_1)\right] R_1^{-n} B_2 = 0. \tag{19}$$

The solvability of the above system (18)-(19) gives

$$a\sigma^2 + b\sigma + c = 0, \tag{20}$$

where

$$\begin{aligned}
a =& -(\mu_1 - \mu_i)(\mu_o - \mu_1)\left(\frac{R_0}{R_1}\right)^n - (\mu_1 + \mu_i)(\mu_o + \mu_1)\left(\frac{R_1}{R_0}\right)^n,\\
b =& \left\{(\mu_1 - \mu_i)\left(\frac{E_1}{nR_1^2} + \frac{Q\mu_1}{2\pi R_1^2}\right) - (\mu_o - \mu_1)\left(\frac{E_0}{nR_0^2} + \frac{Q\mu_1}{2\pi R_0^2}\right)\right\}\left(\frac{R_0}{R_1}\right)^n\\
&+ \left\{(\mu_1 + \mu_i)\left(\frac{E_1}{nR_1^2} - \frac{Q\mu_1}{2\pi R_1^2}\right) + (\mu_o + \mu_1)\left(\frac{E_0}{nR_0^2} - \frac{Q\mu_1}{2\pi R_0^2}\right)\right\}\left(\frac{R_1}{R_0}\right)^n,\\
c =& \left(\frac{E_0}{nR_0^2} + \frac{Q\mu_1}{2\pi R_0^2}\right)\left(\frac{E_1}{nR_1^2} + \frac{Q\mu_1}{2\pi R_1^2}\right)\left(\frac{R_0}{R_1}\right)^n - \left(\frac{E_0}{nR_0^2} - \frac{Q\mu_1}{2\pi R_0^2}\right)\left(\frac{E_1}{nR_1^2} - \frac{Q\mu_1}{2\pi R_1^2}\right)\left(\frac{R_1}{R_0}\right)^n.
\end{aligned}$$

Therefore, $\sigma$ is given by the expression

$$\sigma^{\pm} = \frac{-b \pm \sqrt{b^2 - 4ac}}{2a}. \tag{21}$$

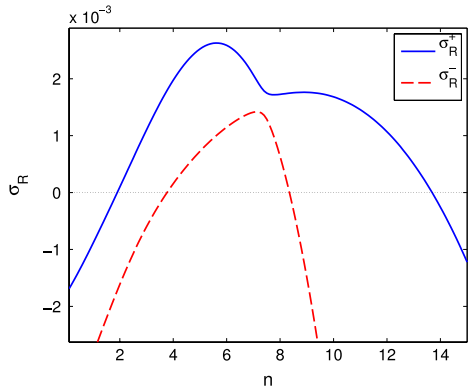


FIG. 4. Plot of the real part of the growth rate $\sigma_R$ versus the wavenumber $n$ for $R_0 = 20$, $R_1 = 30$, $\mu_i = 2$, $\mu_1 = 5$, $\mu_o = 10$, $Q = 10$, $T_0 = 1$, and $T_1 = 1$.

Here, there are two values of the growth rate, $\sigma^+$ and $\sigma^-$, which corresponds to the number of interfaces in the flow. However, it should be stressed that these values do not correspond to the stability of the individual interfaces, but instead characterize the stability of the system as a whole.

A typical plot of the real part of $\sigma$, denoted $\sigma_R$, versus the wavenumber $n$ is given in Figure 4. Here, we used the values $R_0 = 20$, $R_1 = 30$, $\mu_i = 2$, $\mu_1 = 5$, $\mu_o = 10$, $Q = 10$, $T_0 = 1$, and $T_1 = 1$. In this case, $\sigma$ is real for all $n$. Note that both modes are stable for short waves due to interfacial tension. Also, the wave with wavenumber $n = 1$ is stable. It can be shown that when $n = 1$, $a, b, c < 0$ for any values of the parameters. Therefore, the wave whose wavelength is the entire circumference of the interface is always stable. This stands in stark contrast to rectilinear flow in which long waves are unstable. Therefore, we can conclude that the curvature has the effect of stabilizing long waves. We also note that there are exactly two values of $n$ for which $\sigma_R^+ = 0$. We refer to the greater of these values as the maximum neutral wavenumber and the lesser of these as the minimum neutral wavenumber. The difference between these values is the unstable bandwidth. Note that it is possible for $\sigma$ to be complex. The imaginary part of sigma corresponds to the phase speed of the wave. Consider, for example, the values $R_0 = 9$, $R_1 = 11$, $\mu_i = 2$, $\mu_1 = 8$, $\mu_o = 10$, $Q = 1$, $T_0 = 1$, and $T_1 = 1$. Then, for a range of wavenumbers, $\sigma$ is complex. In particular, for $n = 3$ we get $\sigma = -0.0019 \pm 0.0002i$. Figure 5 shows $\sigma_R$ versus the wavenumber $n$. $\sigma$ is complex when the two curves coincide. This is a unique feature of multi-layer radial flows because $\sigma$ is always real for both two-layer radial flow and multi-layer rectilinear flow. Notice that in our example, the complex $\sigma$ has a negative real part. Therefore, this complex growth rate corresponds to a stable wave. We believe this to be the only case in which $\sigma$ is complex.

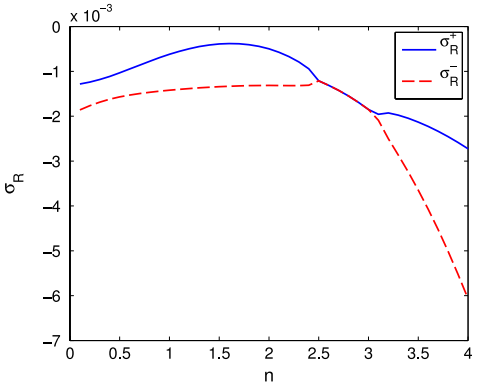


FIG. 5. Plot of the real part of the growth rate $\sigma_R$ versus the wavenumber $n$ for $R_0 = 9$, $R_1 = 11$, $\mu_i = 2$, $\mu_1 = 8$, $\mu_o = 10$, $Q = 1$, $T_0 = 1$, and $T_1 = 1$.

We now consider this solution in some limiting cases. First, consider the thick-layer limit when $R_1 >> R_0$. In this case, the terms that are multiplied by $(R_1/R_0)^n$ dominate those that are multiplied by $(R_0/R_1)^n$. Therefore,

$$a \to -(\mu_1+\mu_i)(\mu_o+\mu_1)\left(\frac{R_1}{R_0}\right)^n, \tag{22}$$

$$b \to \left\{(\mu_1+\mu_i)\left(\frac{E_1}{nR_1^2}-\frac{Q\mu_1}{2\pi R_1^2}\right)+(\mu_o+\mu_1)\left(\frac{E_0}{nR_0^2}-\frac{Q\mu_1}{2\pi R_0^2}\right)\right\}\left(\frac{R_1}{R_0}\right)^n, \tag{23}$$

$$c \to -\left(\frac{E_0}{nR_0^2}-\frac{Q\mu_1}{2\pi R_0^2}\right)\left(\frac{E_1}{nR_1^2}-\frac{Q\mu_1}{2\pi R_1^2}\right)\left(\frac{R_1}{R_0}\right)^n. \tag{24}$$

Using (22)-(24),

$$b^2-4ac \to \left\{(\mu_1+\mu_i)\left(\frac{E_1}{nR_1^2}-\frac{Q\mu_1}{2\pi R_1^2}\right)-(\mu_o+\mu_1)\left(\frac{E_0}{nR_0^2}-\frac{Q\mu_1}{2\pi R_0^2}\right)\right\}^2\left(\frac{R_1}{R_0}\right)^{2n}.$$

We denote $\sigma^+ = (-b+\sqrt{b^2-4ac})/(2a)$ and $\sigma^- = (-b-\sqrt{b^2-4ac})/(2a)$. Then after some algebraic manipulation we obtain

$$\sigma^+ = \frac{Qn}{2\pi R_0^2}\frac{\mu_1-\mu_i}{\mu_1+\mu_i}-\frac{Q}{2\pi R_0^2}-\frac{T_0}{\mu_1+\mu_i}\frac{n\left(n^2-1\right)}{R_0^3}, \tag{25}$$

$$\sigma^- = \frac{Qn}{2\pi R_1^2}\frac{\mu_o-\mu_1}{\mu_o+\mu_1}-\frac{Q}{2\pi R_1^2}-\frac{T_1}{\mu_o+\mu_1}\frac{n\left(n^2-1\right)}{R_1^3}. \tag{26}$$

Note that $\sigma^+$ is the two-layer growth rate at the inner interface and $\sigma^-$ is the two-layer growth rate at the outer interface. This is what we expect since the interfaces do not interact in the thick-layer limit.

Next we consider the thin-layer limit. Fix $R$ and consider the limit as $R_0, R_1 \to R$. Then, in particular, $(R_0/R_1)^n, (R_1/R_0)^n \to 1$ for all $n$. In addition,

$$E_0 \to \frac{Qn^2}{2\pi}(\mu_1-\mu_i)-\frac{Qn}{2\pi}\mu_i-T_0\frac{n^4-n^2}{R}, \tag{27}$$

$$E_1 \to \frac{Qn^2}{2\pi}(\mu_o-\mu_1)-\frac{Qn}{2\pi}\mu_o-T_1\frac{n^4-n^2}{R}, \tag{28}$$

and after some simplification

$$a \to -2\mu_1(\mu_o+\mu_i), \tag{29}$$

$$b \to 2\mu_1\left(\frac{E_0}{nR^2}+\frac{E_1}{nR^2}-\frac{Q}{2\pi R^2}(\mu_o+\mu_i)\right), \tag{30}$$

$$c = 2\mu_1\frac{Q}{2\pi R^2}\left(\frac{E_0}{nR^2}+\frac{E_1}{nR^2}\right). \tag{31}$$

Using (29)-(31)

$$b^2-4ac \to \left\{2\mu_1\left(\frac{E_0}{nR^2}+\frac{E_1}{nR^2}+\frac{Q}{2\pi R^2}(\mu_o+\mu_i)\right)\right\}^2.$$

Then

$$\sigma^+ = \frac{4\mu_1\left\{\frac{Q}{2\pi R^2}(\mu_o+\mu_i)\right\}}{-4\mu_1(\mu_o+\mu_i)} = -\frac{Q}{2\pi R^2}, \tag{32}$$

which is independent of $n$ and stable, and

$$\sigma^- = \frac{Qn}{2\pi R^2}\frac{\mu_o-\mu_i}{\mu_o+\mu_i}-\frac{Q}{2\pi R^2}-\frac{T_0+T_1}{\mu_o+\mu_i}\frac{n\left(n^2-1\right)}{R^3}. \tag{33}$$

This expression is the growth rate of a single interface at $R$ separating fluids with the viscosities of the outer and inner fluids and with its interfacial tension equal to the sum of the interfacial tensions of the two interfaces.

### 2. Upper bounds on the growth rate

To obtain upper bounds on $\sigma_R$ we take the Ordinary Differential Equation (7), multiply by $\left(\sigma + Q/(2\pi r^2)\right)\mu_1 f^*(r)$, and integrate from $R_0$ to $R_1$. Then

$$\int_{R_0}^{R_1} \left(r^3 f'(r)\right)' f^*(r)\left(\sigma\mu_1 + \frac{Q\mu_1}{2\pi r^2}\right)dr - \left(n^2-1\right)\int_{R_0}^{R_1} r|f(r)|^2\left(\sigma\mu_1 + \frac{Q\mu_1}{2\pi r^2}\right)dr = 0.$$

Using integration by parts on the first term and using the interface conditions (14) and (16), we get

$$\begin{aligned}
&\left[E_1 - \frac{Q\mu_1}{2\pi} - \sigma R_1^2(\mu_1 + n\mu_o)\right]|f(R_1)|^2 + \left[E_0 + \frac{Q\mu_1}{2\pi} - \sigma R_0^2(n\mu_i - \mu_1)\right]|f(R_0)|^2 \\
&- \sigma\mu_1\left\{\int_{R_0}^{R_1} r^3|f'(r)|^2dr + \left(n^2-1\right)\int_{R_0}^{R_1} r|f(r)|^2dr\right\} \\
&- \frac{Q\mu_1}{2\pi}\left\{\int_{R_0}^{R_1} r|f'(r)|^2dr + \left(n^2-1\right)\int_{R_0}^{R_1}\frac{|f(r)|^2}{r}dr\right\} + \frac{Q\mu_1}{2\pi}\int_{R_0}^{R_1} 2f'(r)f^*(r)dr = 0.
\end{aligned} \tag{34}$$

But note that

$$\left(|f(r)|^2\right)' = \left(f(r)f^*(r)\right)' = f'(r)f^*(r) + f(r)\left(f^*(r)\right)'. \tag{35}$$

Therefore,

$$\begin{aligned}
\int_{R_0}^{R_1} 2f'(r)f^*(r)dr &= \int_{R_0}^{R_1}\left(|f(r)|^2\right)' + f'(r)f^*(r) - f(r)\left(f^*(r)\right)'dr \\
&= |f(R_1)|^2 - |f(R_0)|^2 + \int_{R_0}^{R_1} f'(r)f^*(r) - f(r)\left(f^*(r)\right)'dr.
\end{aligned}$$

Using this expression in (34) and solving the resulting equation for $\sigma$ gives

$$\sigma = \frac{E_0|f(R_0)|^2 + E_1|f(R_1)|^2 + \frac{Q\mu_1}{2\pi}I_0 - \frac{Q\mu_1}{2\pi}I_1}{R_0^2(n\mu_i - \mu_1)|f(R_0)|^2 + R_1^2(\mu_1 + n\mu_o)|f(R_1)|^2 + \mu_1 I_2}, \tag{36}$$

where

$$I_0 = \int_{R_0}^{R_1} f'(r)f^*(r) - f(r)\left(f^*(r)\right)'dr, \tag{37}$$

$$I_1 = \int_{R_0}^{R_1}\left(r|f'(r)|^2 + \left(n^2-1\right)\frac{|f(r)|^2}{r}\right)dr, \tag{38}$$

$$I_2 = \int_{R_0}^{R_1}\left(r^3|f'(r)|^2 + \left(n^2-1\right)r|f(r)|^2\right)dr. \tag{39}$$

Note that $I_1$ and $I_2$ are both real and positive for a non-zero $f(r)$. Also note that the integrand of $I_0$ is the difference of complex conjugates and is thus purely imaginary. Let $\sigma_R$ denote the real part of $\sigma$ and $\sigma_i$ denote the imaginary part. Then

$$\sigma_R = \frac{E_0|f(R_0)|^2 + E_1|f(R_1)|^2 - \frac{Q\mu_1}{2\pi}I_1}{R_0^2(n\mu_i - \mu_1)|f(R_0)|^2 + R_1^2(\mu_1 + n\mu_o)|f(R_1)|^2 + \mu_1 I_2} \tag{40}$$

and

$$i\sigma_i = \frac{\frac{Q\mu_1}{2\pi}I_0}{R_0^2(n\mu_i - \mu_1)|f(R_0)|^2 + R_1^2(\mu_1 + n\mu_o)|f(R_1)|^2 + \mu_1 I_2}. \tag{41}$$

We wish to bound $\sigma_R$. We do this by invoking the following lemma.

*Lemma 1. Let $f(r)$ solve the differential equation (7) and $I_2$ be defined by (39). Then*

$$I_2 \geq n\, g(R_0,R_1)\Big(\lambda_1 R_0^2|f(R_0)|^2 + \lambda_2 R_1^2|f(R_1)|^2\Big) + R_0^2|f(R_0)|^2 - R_1^2|f(R_1)|^2, \tag{42}$$

*where*

$$g(r,s) = \frac{\left(\frac{s}{r}\right)^n - \left(\frac{r}{s}\right)^n}{\left(\frac{s}{r}\right)^n + \left(\frac{r}{s}\right)^n}, \tag{43}$$

*for any $\lambda_1, \lambda_2 > 0$ such that $\lambda_1 + \lambda_2 \leq 1$.*

*Proof.* If $f(r)$ solves (7), then

$$\left(r^3 f'(r)\right)' = \left(n^2 - 1\right) r f(r).$$

Using the product rule,

$$\left(r^3 f'(r) f^*(r)\right)' = r^3|f'(r)|^2 + \left(r^3 f'(r)\right)' f^*(r) = r^3|f'(r)|^2 + \left(n^2-1\right) r|f(r)|^2.$$

Therefore,

$$I_2 = \int_{R_0}^{R_1} \left(r^3 f'(r) f^*(r)\right)' dr = R_1^3 f'(R_1) f^*(R_1) - R_0^3 f'(R_0) f^*(R_0). \tag{44}$$

The solution to (7) can be written as

$$f(r) = \frac{\left[f(R_1)\left(\frac{R_0}{R_1}\right)^{n-1} - f(R_0)\right]\left(\frac{r}{R_0}\right)^{-n-1} + \left[f(R_0)\left(\frac{R_0}{R_1}\right)^{n+1} - f(R_1)\right]\left(\frac{r}{R_1}\right)^{n-1}}{\left(\frac{R_0}{R_1}\right)^{2n} - 1}. \tag{45}$$

Using expressions for $f'(R_0)$ and $f'(R_1)$ derived from (45) in equation (44) and then after some algebraic manipulation, we get

$$I_2 = \frac{n(R_1^2|f(R_1)|^2 + R_0^2|f(R_0)|^2)}{g(R_0,R_1)} - \frac{2nR_0R_1[f^*(R_0)f(R_1) + f(R_0)f^*(R_1)]}{\left(\frac{R_1}{R_0}\right)^n - \left(\frac{R_0}{R_1}\right)^n} + R_0^2|f(R_0)|^2 - R_1^2|f(R_1)|^2,$$

where $g(\cdot,\cdot)$ has been defined in (43). But

$$f^*(R_0)f(R_1) + f(R_0)f^*(R_1) = 2Re(f(R_0)f^*(R_1)) \leq 2|f(R_0)||f(R_1)|.$$

Therefore,

$$I_2 > \frac{n(R_1^2|f(R_1)|^2 + R_0^2|f(R_0)|^2)}{g(R_0,R_1)} - \frac{4nR_0R_1|f(R_0)||f(R_1)|}{\left(\frac{R_1}{R_0}\right)^n - \left(\frac{R_0}{R_1}\right)^n} + R_0^2|f(R_0)|^2 - R_1^2|f(R_1)|^2.$$

Let $b = \ln\left(\left(\frac{R_1}{R_0}\right)^n\right)$, $\zeta = R_0|f(R_0)|$, and $\chi = R_1|f(R_1)|$. Then

$$I_2 > n\, F(\zeta,\chi) + \zeta^2 - \chi^2, \tag{46}$$

where

$$F(\zeta,\chi) = \frac{1}{\sinh(b)}\left\{\zeta^2\cosh(b) - 2\zeta\chi + \chi^2\cosh(b)\right\}.$$

We recall from Daripa[23] the following result:

$$F(\zeta,\chi) \geq \tanh(b)(\lambda_1\zeta^2 + \lambda_2\chi^2),$$

which holds for any $\lambda_1 + \lambda_2 \leq 1$. Inserting this equality in (46), we obtain

$$I_2 \geq n\tanh(b)\left(\lambda_1\zeta^2 + \lambda_2\chi^2\right) + \zeta^2 - \chi^2.$$

By reinserting the values of $b$, $\zeta$, and $\chi$, we obtain Lemma 1. □

We now use this inequality in expression (40). Since the denominator is now positive, we may also ignore the negative term in the numerator. Therefore,

$$\sigma_R < \frac{E_0|f(R_0)|^2 + E_1|f(R_1)|^2}{nR_0^2(\mu_i + \mu_1\lambda_1 g(R_0,R_1))\,|f(R_0)|^2 + nR_1^2(\mu_o + \mu_1\lambda_2 g(R_0,R_1))\,|f(R_1)|^2}.$$

We consider four cases:

1. If $E_0 < 0$ and $E_1 < 0$, then $\sigma_R < 0$.
2. If $E_0 < 0$ and $E_1 > 0$, then we can neglect the negative term $E_0|f(R_0)|^2$ in the numerator and the corresponding positive term in the denominator to get
$$\sigma_R < \frac{E_1}{nR_1^2(\mu_o + \mu_1\lambda_2 g(R_0,R_1))}.$$
3. If $E_0 > 0$ and $E_1 < 0$, we neglect the negative term $E_1|f(R_1)|^2$ in the numerator and the corresponding positive term in the denominator to get
$$\sigma_R < \frac{E_0}{nR_0^2(\mu_i + \mu_1\lambda_1 g(R_0,R_1))}.$$
4. If $E_0 > 0$ and $E_1 > 0$, then all terms are positive. We use the following inequality which holds for any $N$ if $A_i > 0$, $B_i > 0$, and $X_i > 0$ for all $i = 1,\ldots,N$. Then
$$\frac{\sum_{i=1}^{N} A_i X_i}{\sum_{i=1}^{N} B_i X_i} \le \max_i \left\{\frac{A_i}{B_i}\right\}.$$
By using this inequality with $N = 2$, we get

$$\sigma_R < \max\left(\frac{E_0}{nR_0^2(\mu_i + \mu_1\lambda_1 g(R_0,R_1))}, \frac{E_1}{nR_1^2(\mu_o + \mu_1\lambda_2 g(R_0,R_1))}\right). \tag{47}$$

Clearly, the upper bound (47) holds for the second and third cases above. Therefore, it holds for all unstable modes.

We now see the results for several different combinations of $\lambda_1$ and $\lambda_2$. First, consider $\lambda_1 = \lambda_2 = 0$. Note that this minimizes the denominator and thus gives the worst possible upper bound among all choices of $\lambda_i's$. This choice yields the upper bound

$$\sigma_R < \max\left(\frac{E_0}{nR_0^2\mu_i}, \frac{E_1}{nR_1^2\mu_o}\right). \tag{48}$$

Then it is easily seen from the maximum value that each of the two terms take over all waves that the absolute upper bound is given by

$$\sigma_R^u = \max\left\{\left[\frac{Qn_0}{2\pi R_0^2}\left(\frac{\mu_1 - \mu_i}{\mu_i}\right) - \frac{Q}{2\pi R_0^2} - T_0\frac{n_0^3 - n_0}{R_0^3}\frac{1}{\mu_i}\right], \left[\frac{Qn_1}{2\pi R_1^2}\left(\frac{\mu_o - \mu_1}{\mu_o}\right) - \frac{Q}{2\pi R_1^2} - T_1\frac{n_1^3 - n_1}{R_1^3}\frac{1}{\mu_o}\right]\right\}, \tag{49}$$

where $n_0 = \sqrt{QR_0(\mu_1 - \mu_i)/(6\pi T_0) + 1/3}$ and $n_1 = \sqrt{QR_1(\mu_o - \mu_1)/(6\pi T_1) + 1/3}$. Compare these values to the value of $n_m$ in the case of two-layer flow (see Sec. II). Note that $n_0$ and $n_1$ correspond to the values of $n_m$ for flows with only the inner and outer interface, respectively. We find that the absolute upper bound is minimized by the choice of interfacial tensions

$$T_0 = \frac{QR_0(\mu_1 - \mu_i)}{4\pi}, \qquad T_1 = \frac{QR_1(\mu_o - \mu_1)}{4\pi}. \tag{50}$$

As in the two-layer case, these values of $T_0$ and $T_1$ are the values of interfacial tension that correspond to $n_0 = n_1 = 1$. Therefore, for all values of $T_0$ and $T_1$ that are greater than the expressions given in (50) will have $n = 1$ as their most unstable wave and the absolute upper bound will become

$$\sigma_R^u = \max\left\{\left[\frac{Q}{2\pi R_0^2}\left(\frac{\mu_1 - 2\mu_i}{\mu_i}\right)\right], \left[\frac{Q}{2\pi R_1^2}\left(\frac{-\mu_1}{\mu_o}\right)\right]\right\} \tag{51}$$

which is independent of $T_0$ and $T_1$ and negative whenever $\mu_1 < 2\mu_i$.

For improved estimates, we can choose nonzero values for $\lambda_i$. Of particular interest is $\lambda_1 = 1$ and $\lambda_2 = 0$, which minimizes the term corresponding to the inner interface. This gives the upper bound

$$\sigma_R < \max\left(\frac{E_0}{nR_0^2(\mu_i + \mu_1 g(R_0, R_1))}, \frac{E_1}{nR_1^2\mu_o}\right). \tag{52}$$

Conversely, we can consider $\lambda_1 = 0$ and $\lambda_2 = 1$ which minimizes the term corresponding to the outer interface and get

$$\sigma_R < \max\left(\frac{E_0}{nR_0^2\mu_i}, \frac{E_1}{nR_1^2(\mu_o + \mu_1 g(R_0, R_1))}\right). \tag{53}$$

Note that both $\sigma^+$ and $\sigma^-$ given by (21) will satisfy these upper bounds.

### B. Multi-layer flows

We now consider the case of an arbitrary number of fluid layers (see Figure 6). Let there be $N$ intermediate layers of fluid—and thus $N + 2$ total layers of fluid—with $N + 1$ interfaces at $R_0 < R_1 < \cdots < R_{N-1} < R_N$. The respective interfacial tensions are $T_0, \ldots, T_N$. As before, the fluid in the inner region has viscosity $\mu_i$ and the fluid in the outer region has viscosity $\mu_o$. For j = 1, ... N, the fluid in the annulus $R_{j-1} < r < R_j$ has viscosity $\mu_j$. We assume that $\mu_i < \mu_1 < \mu_2 < \cdots < \mu_N < \mu_o$.

Equation (7) holds within each layer of fluid. Therefore, the solution, $f(r)$, is of the form

$$f(r) = \begin{cases} A_0 r^{n-1} + B_0 r^{-(n+1)}, & r < R_0 \\ A_j r^{n-1} + B_j r^{-(n+1)}, & R_{j-1} < r < R_j, \quad 1 \le j \le N \\ A_{N+1} r^{n-1} + B_{N+1} r^{-(n+1)}, & r > R_N \end{cases}, \tag{54}$$

where the interface conditions are given by equation (11) at each $r = R_j$. As in the three-layer problem, we require that $B_0 = 0$ and $A_{N+1} = 0$ so that the disturbances go to zero as $r \to \infty$, and

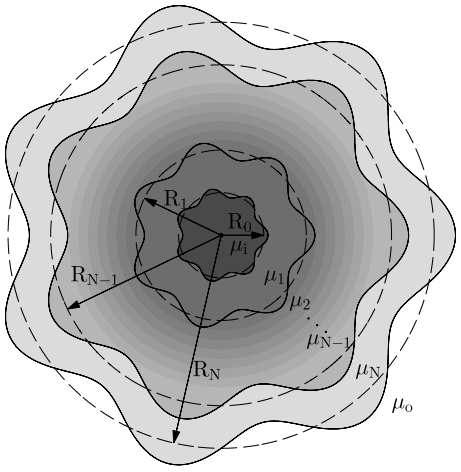


FIG. 6. N-layer flow.

there is no singularity at $r = 0$. Using (54) in (11) leads to the following expressions for the interface conditions on the inner and outermost interfaces:

$$\left(\sigma + \frac{Q}{2\pi R_0^2}\right)\mu_1 R_0^3 (f^+)'(R_0) = -\left[E_0 + \frac{Q\mu_1}{2\pi} - \sigma R_0^2(n\mu_i - \mu_1)\right] f(R_0), \tag{55}$$

$$\left(\sigma + \frac{Q}{2\pi R_N^2}\right)\mu_N R_N^3 (f^-)'(R_N) = \left[E_N - \frac{Q\mu_N}{2\pi} - \sigma R_N^2(\mu_N + n\mu_o)\right] f(R_N), \tag{56}$$

where

$$E_0 = \frac{Qn^2}{2\pi}(\mu_1 - \mu_i) - \frac{Qn}{2\pi}\mu_i - T_0\frac{n^4 - n^2}{R_0}, \quad E_N = \frac{Qn^2}{2\pi}(\mu_o - \mu_N) - \frac{Qn}{2\pi}\mu_o - T_N\frac{n^4 - n^2}{R_N}.$$

For the intermediate interfaces, we have for $j = 1, \ldots, N-1$

$$\begin{aligned}&\left(\sigma + \frac{Q}{2\pi R_j^2}\right) R_j^3(\mu_j (f^-)'(R_j) - \mu_{j+1}(f^+)'(R_j)) \\ &= \left[E_j + \frac{Q}{2\pi}(\mu_{j+1} - \mu_j) + \sigma R_j^2(\mu_{j+1} - \mu_j)\right] f(R_j),\end{aligned} \tag{57}$$

where

$$E_j = \frac{Qn^2}{2\pi}(\mu_{j+1} - \mu_j) - T_j\frac{n^4 - n^2}{R_j}.$$

Note that there are $(2N + 2)$ constants to be determined in equation (54). The function $f(r)$ must be continuous across each of the $N + 1$ interfaces. This leaves $N + 1$ free constants. The set of $N + 1$ interface conditions gives a system of the form $\mathbf{Ax} = 0$ where $\mathbf{x}$ is a vector of length $N + 1$ and $\mathbf{A}$ is a square matrix. For this equation to have nontrivial solutions, we need $det(A) = 0$. Since the interface conditions are linear in $\sigma$, this results in an $N + 1$ degree polynomial for $\sigma$. Therefore, there are at most $N + 1$ distinct values of $\sigma$ for each wavenumber $n$.

We now return to equation (7) which holds for $R_{j-1} < r < R_j$ for any $1 \le j \le N$. We multiply by $\left(\sigma + Q/(2\pi r^2)\right)\mu_j f^*(r)$ and integrate from $R_{j-1}$ to $R_j$ to get

$$\int_{R_{j-1}}^{R_j} \left(\left(r^3 f'(r)\right)' f^*(r) - \left(n^2 - 1\right) r|f(r)|^2\right)\left(\sigma\mu_j + \frac{Q\mu_j}{2\pi r^2}\right) dr = 0.$$

Following the procedure from the three-layer case, we use integration by parts on the first term and insert the interface conditions. Then we sum these expressions over all values of $j$ to get

$$\begin{aligned}&\left[E_0 + \frac{Q\mu_1}{2\pi} - \sigma R_0^2(\mu_1 - n\mu_i)\right]|f(R_0)|^2 \\ &+ \sum_{j=1}^{N-1}\left[E_j + \frac{Q}{2\pi}(\mu_{j+1} - \mu_j) + \sigma R_j^2(\mu_{j+1} - \mu_j)\right]|f(R_j)|^2 \\ &+ \left[E_N - \frac{Q\mu_N}{2\pi} - \sigma R_N^2(\mu_N + n\mu_o)\right]|f(R_N)|^2 \\ &- \sum_{j=1}^{N}\left\{\mu_j\int_{R_{j-1}}^{R_j} r^3|f'(r)|^2\left(\sigma + \frac{Q}{2\pi r^2}\right)dr\right\} + \frac{Q}{2\pi}\sum_{j=1}^{N}\left\{\mu_j\int_{R_{j-1}}^{R_j} 2f'(r)f^*(r)dr\right\} \\ &- \sum_{j=1}^{N}\left\{\left(n^2 - 1\right)\int_{R_{j-1}}^{R_j} r|f(r)|^2\left(\sigma + \frac{Q}{2\pi r^2}\right)dr\right\} = 0.\end{aligned}$$

Using that

$$\int_{R_{j-1}}^{R_j} 2f'(r)f^*(r)dr = |f(R_j)|^2 - |f(R_{j-1})|^2 + \int_{R_{j-1}}^{R_j} f'(r)f^*(r) - f(r)(f^*(r))'dr$$

and solving for $\sigma$ gives the expression

$$\sigma = \frac{\sum_{j=0}^{N} E_j |f(R_j)|^2 + \frac{Q}{2\pi} J_0 - \frac{Q}{2\pi} J_1}{\sum_{j=0}^{N} F_j |f(R_j)|^2 + J_2}, \tag{58}$$

where $F_0 = R_0^2(n\mu_i - \mu_1)$, $F_j = R_j^2(\mu_j - \mu_{j+1})$ for $1 \le j \le N-1$, $F_N = R_N^2(\mu_N + n\mu_o)$ and

$$\begin{aligned}
J_0 &= \sum_{j=1}^{N} \left\{ \mu_j \int_{R_{j-1}}^{R_j} f'(r) f^*(r) - f(r)(f^*(r))' dr \right\}, \\
J_1 &= \sum_{j=1}^{N} \left\{ \mu_j \int_{R_{j-1}}^{R_j} \left( r|f'(r)|^2 + \left(n^2 - 1\right) \frac{|f(r)|^2}{r} \right) dr \right\}, \\
J_2 &= \sum_{j=1}^{N} \left\{ \mu_j \int_{R_{j-1}}^{R_j} \left( r^3 |f'(r)|^2 + \left(n^2 - 1\right) r |f(r)|^2 \right) dr \right\}.
\end{aligned}$$

Again, $J_0$ is the difference of complex conjugates and is purely imaginary. Therefore,

$$\sigma_R = \frac{\sum_{j=0}^{N} E_j |f(R_j)|^2 - \frac{Q}{2\pi} J_1}{\sum_{j=0}^{N} F_j |f(R_j)|^2 + J_2}. \tag{59}$$

Lemma 1 implies that for any $j = 1, \ldots, N$,

$$\begin{aligned}
&\int_{R_{j-1}}^{R_j} \left( r^3 |f'(r)|^2 + (n^2 - 1) r |f(r)|^2 \right) dr \\
&\ge n\, g(R_{j-1}, R_j) \Big( \lambda_{j,1} R_{j-1}^2 |f(R_{j-1})|^2 + \lambda_{j,2} R_j^2 |f(R_j)|^2 \Big) + R_{j-1}^2 |f(R_{j-1})|^2 - R_j^2 |f(R_j)|^2,
\end{aligned}$$

for any $\lambda_{j,1}, \lambda_{j,2} \ge 0$ such that $\lambda_{j,1} + \lambda_{j,2} \le 1$, where $g(\cdot,\cdot)$ has been defined in (43). Therefore,

$$\begin{aligned}
J_2 \ge{}& \Big( \lambda_{1,1} \mu_1\, n\, g(R_0, R_1) R_0^2 + \mu_1 R_0^2 \Big) |f(R_0)|^2 \\
&+ \sum_{j=1}^{N-1} R_j^2 \Big( \lambda_{j,2} \mu_j\, n\, g(R_{j-1}, R_j) + \lambda_{j+1,1} \mu_{j+1}\, n\, g(R_j, R_{j+1}) + (\mu_{j+1} - \mu_j) \Big) |f(R_j)|^2 \\
&+ \Big( \lambda_{N,2} \mu_N\, n\, g(R_{N-1}, R_N) R_N^2 - \mu_N R_N^2 \Big) |f(R_N)|^2.
\end{aligned}$$

Using this expression in place of $J_2$ and ignoring the negative integral term in the numerator, we get

$$\sigma_R < \frac{\sum_{j=0}^{N} E_j |f(R_j)|^2}{\sum_{j=0}^{N} n R_j^2 G_j |f(R_j)|^2}, \tag{60}$$

where

$$\begin{aligned}
G_0 &= \lambda_{1,1} \mu_1 g(R_0, R_1) + \mu_i, \\
G_j &= \lambda_{j,2} \mu_j g(R_{j-1}, R_j) + \lambda_{j+1,1} \mu_{j+1} g(R_j, R_{j+1}), \qquad 1 \le j \le N-1 \\
G_N &= \lambda_{N,2} \mu_N g(R_{N-1}, R_N) + \mu_o
\end{aligned}$$

for any choice of $\lambda_{j,k}$'s such that $\lambda_{j_1} + \lambda_{j_2} \leq 1$ for all $j$. In particular this means that for all unstable modes,

$$\sigma_R < \max_{0\leq j\leq N}\left(\frac{E_j}{nR_j^2G_j}\right). \tag{61}$$

Note that when $N = 1$, this corresponds with the three-layer upper bound, (47), where $\lambda_1 = \lambda_{1,1}$ and $\lambda_2 = \lambda_{N,2}$.

## C. Special cases

In this section, we show how to construct appropriate limits in order to recover well-known results for rectilinear flows and a special case for radial flows. This analysis in turn establishes a connection between instabilities in radial and rectilinear geometries.

### 1. Connection to rectilinear flow

The curvature of the interface is an important physical aspect of this radial flow configuration. However, as more fluid is injected into the cell, the curvatures of the interfaces decrease. In particular, as the radius of a circular interface goes to infinity, the curvature goes to zero. Additionally, since an interface at $R_j$ moves with velocity $Q/(2\pi R_j)$, the inner interfaces move faster than the outer interfaces. Therefore, if interfaces are located at $R_j$ and $R_k$, then the ratio $R_j/R_k$ approaches 1 as more fluid is pumped into the cell.

In light of this information, we investigate the zero curvature limit. Let $R_j \to \infty$ for $0 \leq j \leq N$ such that $R_j/R_k \to 1$ for all $0 \leq j,k \leq N$ and also $Q, n \to \infty$ such that $Q/(2\pi R_0)$ and $n/R_0$ are constants. We denote these constants by $U$ and $k$, respectively. Note in particular that since $R_0/R_j \to 1$ for all $j$, $Q/(2\pi R_j) \to U$ and $n/R_j \to k$. The equation (7) is rewritten as

$$f''(r) + \frac{3}{r}f'(r) + \frac{1-n^2}{r^2}f(r) = 0.$$

In any of the intermediate layers, we will have $R_0 < r < R_N$. Therefore, $r \to \infty$ such that $n/r \to k$. Taking this limit, we are left with

$$f''(r) - k^2 f(r) = 0. \tag{62}$$

Now consider the boundary condition (11) at $R = R_j$ and divide by $R_j^3$. Then

$$\left(\sigma + \frac{Q}{2\pi R_j^2}\right)\{\mu^-(f^-)'(R_j) - \mu^+(f^+)'(R_j)\}$$
$$= \left\{\left(\frac{\sigma}{R_j} + \frac{Q}{2\pi R_j^3}\right)(\mu^+ - \mu^-) + \frac{Qn^2}{2\pi R_j^3}(\mu^+ - \mu^-) - T_j\frac{n^4 - n^2}{R_j^4}\right\} f(R_j).$$

Taking the prescribed limits gives

$$\sigma\{\mu^-(f^-)'(R_j) - \mu^+(f^+)'(R_j)\} = \{Uk^2(\mu^+ - \mu^-) - T_jk^4\} f(R_j).$$

Therefore,

$$\mu^-(f^-)'(R_j)f(R_j) - \mu^+(f^+)'(R_j)f(R_j) = \frac{Uk^2(\mu^+ - \mu^-) - T_jk^4}{\sigma}|f(R_j)|^2. \tag{63}$$

Equations (62) and (63) agree with the equations derived by Daripa[23] for rectilinear flow in a Hele-Shaw cell.

Next, consider a three-layer radial flow. Recall that $\sigma$ is the solution to a quadratic equation $a\sigma^2 + b\sigma + c = 0$ given by (20). We now require that $R_0/R_1 = exp(-L/R_0)$ for some constant $L$. This ensures that $R_0/R_1 \to 1$ as $R_0, R_1 \to \infty$. Then, $(R_0/R_1)^n = exp(-nL/R_0) = exp(-kL)$. Using

this limit along with the previously imposed limits, we get

$$\begin{aligned} a &= e^{-kL}(\mu-\mu_i)(\mu-\mu_o) - e^{kL}(\mu+\mu_i)(\mu_o+\mu), \\ b &= \left[e^{kL}(\mu+\mu_i) + e^{-kL}(\mu-\mu_i)\right]\xi - \left[e^{kL}(\mu_o+\mu) + e^{-kL}(\mu-\mu_o)\right]\tau, \\ c &= \tau\xi(e^{kL} - e^{-kL}), \end{aligned}$$

where $\tau = -\left[Uk(\mu-\mu_i) - T_0k^3\right]$ and $\xi = \left[Uk(\mu_o-\mu) - T_1k^3\right]$. This agrees with the exact solution found for rectilinear flow by Daripa.[24]

### 2. Stable inner interface

Recall from equation (9) that the amplitude of the disturbance of an interface at $r = R$ at any time $t$ is given by

$$\frac{f(R)}{\sigma + \frac{Q}{2\pi R^2}} e^{\int_0^t \sigma(s)ds}.$$

Therefore, imposing the condition $f(R) = 0$ gives a completely stable interface. Consider three-layer flow in which the inner interface is stable. This is a reasonable assumption if $\mu_i >> \mu_1$. The new eigenvalue problem is defined by

$$\begin{cases} \left(r^3 f'(r)\right)' - \left(n^2-1\right) r f(r) = 0, \quad R_0 \le r \le R_1, \\ f(R_0) = 0, \\ \left(\sigma + \dfrac{Q}{2\pi R_1^2}\right)\mu_1 R_1^3 (f^-)'(R_1) = \left[E_1 - \dfrac{Q\mu_1}{2\pi} - \sigma R_1^2(\mu_1 + n\mu_o)\right] f(R_1). \end{cases} \tag{64}$$

A solution that satisfies the interface condition at $r = R_0$ must take the form

$$f(r) = \frac{C}{R_0^n} r^{n-1} - C R_0^n r^{-(n+1)}$$

for some constant $C$. Plugging this into the interface condition $(64)_3$, we get

$$\begin{aligned} &\left(\sigma + \frac{Q}{2\pi R_1^2}\right)\mu_1 R_1 \left\{(n-1)\left(\frac{R_1}{R_0}\right)^n + (n+1)\left(\frac{R_0}{R_1}\right)^n\right\} \\ &= \left[\frac{E_1}{R_1} - \frac{Q\mu_1}{2\pi R_1} - \sigma R_1(\mu_1 + n\mu_o)\right]\left\{\left(\frac{R_1}{R_0}\right)^n - \left(\frac{R_0}{R_1}\right)^n\right\}, \end{aligned}$$

where $E_1$ is given by (17). Solving for $\sigma$ gives

$$\sigma = -\frac{Q}{2\pi R_1^2} + \frac{\frac{Qn}{2\pi R_1^2}(\mu_o - \mu_i) - T_1\frac{n^3-n}{R_1^3}}{\mu_1\frac{\left(\frac{R_1}{R_0}\right)^n + \left(\frac{R_0}{R_1}\right)^n}{\left(\frac{R_1}{R_0}\right)^n - \left(\frac{R_0}{R_1}\right)^n} + \mu_o},$$

which agrees with the result obtained by Cardoso and Woods.[11]

## IV. STABILIZATION

We now show that the flow may be stabilized by the addition of many layers of fluid with small positive jumps in viscosity. First, we consider the upper bound (60) with $\lambda_{j,k} = 0$ for all j and k. Then $G_j = 0$ for $1 \le j \le N-1$ and

$$\sigma_R < \frac{\sum_{j=0}^N E_j |f(R_j)|^2}{nR_0^2\mu_i|f(R_j)|^2 + nR_N^2\mu_o|f(R_j)|^2}.$$

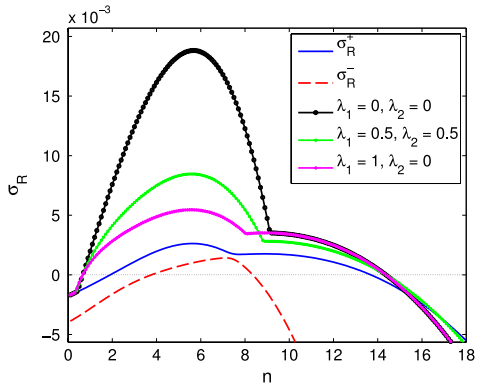


FIG. 7. Plots of exact dispersion relations and the upper bounds (see Eq. (47)) of the growth rate for several different values of $\lambda_1$ and $\lambda_2$. The parameter values are $R_0 = 20$, $R_1 = 30$, $\mu_i = 2$, $\mu_1 = 5$, $\mu_o = 10$, $Q = 10$, $T_0 = 1$, and $T_1 = 1$.

We now use the following fact: If $E_j < 0$ for $1 \le j \le N-1$, then

$$\begin{aligned}\sigma_R &< \max\left\{\frac{E_0}{nR_0^2\mu_i}, \frac{E_N}{nR_N^2\mu_o}\right\}\\ &< \max\left\{\left(\frac{Qn}{2\pi R_0^2}\left(\frac{\mu-\mu_i}{\mu_i}\right) - \frac{Q}{2\pi R_0^2} - T_0\frac{n^3-n}{R_0^3}\frac{1}{\mu_i}\right),\right.\\ &\qquad \left.\left(\frac{Qn}{2\pi R_N^2}\left(\frac{\mu_o-\mu}{\mu_o}\right) - \frac{Q}{2\pi R_N^2} - T_N\frac{n^3-n}{R_N^3}\frac{1}{\mu_o}\right)\right\},\end{aligned}$$

where $\mu$ is any value such that $\mu_1 \le \mu \le \mu_N$. The last inequality above follows since $\mu_1 - \mu_i \le \mu - \mu_i$ and $\mu_o - \mu_N \le \mu_o - \mu$. This is the three-layer upper bound when the intermediate layer viscosity is $\mu$. Therefore, this is an improvement over the three-layer upper bound if $E_j < 0$ for $1 \le j \le N-1$. We consider these terms. Recall that

$$E_j = \frac{Qn^2}{2\pi}(\mu_{j+1} - \mu_j) - T_j\frac{n^4-n^2}{R_j}.$$

We investigate the zeros of this function. The only nonzero values of $n$ for which $E_j = 0$ occur when $Q(\mu_{j+1} - \mu_j)/2\pi - T_j(n^2-1)/R_j = 0$. The positive value of $n$ that satisfies this, which we denote $n_j$, is given by $n_j = \sqrt{QR_j(\mu_{j+1} - \mu_j)/(2\pi T_j) + 1}$. By observing that $E_j$ is negative for large enough $n$, we can deduce that $E_j < 0$ for all $n > n_j$. Note that $E_j > 0$ for $n = 1$ whenever $\mu_{j+1} - \mu_j > 0$. However, by choosing sufficiently small jumps in viscosity at the intermediate interfaces, we can ensure that $E_j < 0$ for all $n \ge 2$. In particular, this is true when $n_j < 2$. This is satisfied when

$$(\mu_{j+1} - \mu_j) < \frac{6\pi T_j}{QR_j}. \tag{65}$$

Note that this expression does not depend on the thickness of the layer. Therefore, we can include many thin layers, each with a small jump in viscosity. To see this, consider the situation in which the innermost interface is at $R_0$ and the outermost interface is at $R_N$ (where the value of $N$ is yet to be determined). We fix some values for $\mu_1$ and $\mu_N$ . We assume that the minimum value of interfacial tension between any two layers of fluid is given by some number $T = \min T_j$. Then, let N be the unique integer such that

$$(N-2) < \frac{(\mu_N - \mu_1)QR_N}{6\pi T} \le (N-1). \tag{66}$$

Then, we let

$$R_j = R_0 + \left(\frac{R_N - R_0}{N}\right)j, \quad 1 \le j \le N-1, \tag{67}$$

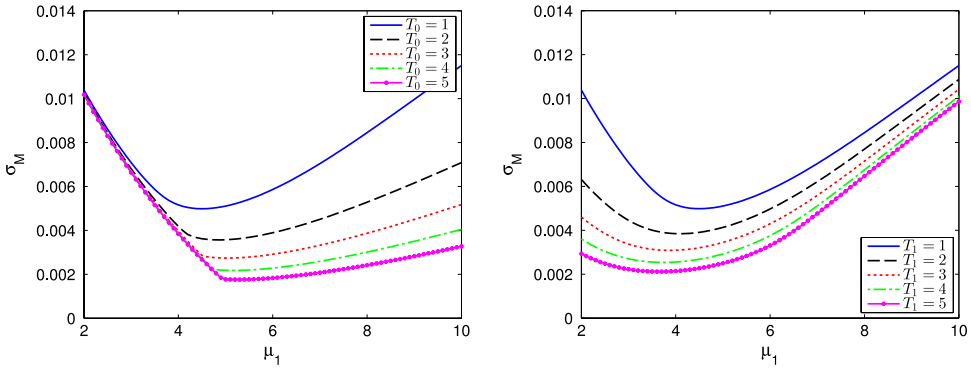


FIG. 8. A plot of the maximum value of the growth rate (see Eq. (21)) versus the viscosity of the intermediate layer, $\mu_1$. In the left plot, $T_1$ is held constant at $T_1 = 1$ while $T_0$ varies. In the right plot, $T_0$ is held constant at $T_0 = 1$ while $T_1$ varies. The other parameter values are $R_0 = 20$, $R_1 = 22$, $\mu_i = 2$, $\mu_o = 10$, and $Q = 10$.

$$\mu_{j+1} = \mu_j + \frac{6\pi T}{QR_N}, \quad 1 \le j \le N-2. \tag{68}$$

Since, $6\pi T/(QR_N) < 6\pi T_j/(QR_j)$ for all $1 \le j \le N-1$, it is clear that (68) ensures that $(\mu_{j+1} - \mu_j) < 6\pi T_j/(QR_j)$ for $1 \le j \le N-2$. It remains to show that this holds for the interface between the fluids of viscosity $\mu_{N-1}$ and $\mu_N$. Note that (68) can be rewritten as $\mu_{j+1} = \mu_1 + 6\pi T j/(QR_N)$. Therefore, $\mu_{N-1} = \mu_1 + (N-2)6\pi T/(QR_N)$. Using this equality, (66), and some algebraic manipulation one obtains $0 < \mu_N - \mu_{N-1} < 6\pi T/(QR_N)$. Therefore, (65) holds for all $1 \le j \le N-1$, and this system has the property that $E_j < 0$ for all $n \ge 2$. Since this can be done for arbitrary values of $\mu_1$ and $\mu_N$, we may choose these values to be such that the destabilizing terms $(Qn/2\pi R_0^2)((\mu_1 - \mu_i)/\mu_i)$ and $(Qn/2\pi R_N^2)((\mu_o - \mu_N)/\mu_o)$ in the upper bounds are arbitrarily small.

As an example of this procedure, consider the values $Q = 10$, $\mu_i = 2$, $\mu_o = 10$, $R_0 = 20$, and $R_N = 30$. We choose fluids for the innermost and outermost intermediate layers so that $\mu_1 = 2.05$, $\mu_N = 9.96$, and $T_0 = T_N = 1$. With these choices, the terms $E_0$ and $E_N$ will be negative for all $n \ge 1$. If all other fluids can be chosen so that $T_j \ge 1$ for all $j$, then, according to equation (66), $N = 127$. Using 128 evenly spaced interfaces with radii given by (67) and fluid viscosity jumps of $\pi/50 \approx 0.063$, $E_j < 0$ for all $1 \le j \le N-1$ and $n \ge 2$.

## V. NUMERICAL RESULTS

We now use the dispersion relation that we found in Sec. III A 1 to numerically investigate the effect of different parameters on the growth rate in three-layer flow.

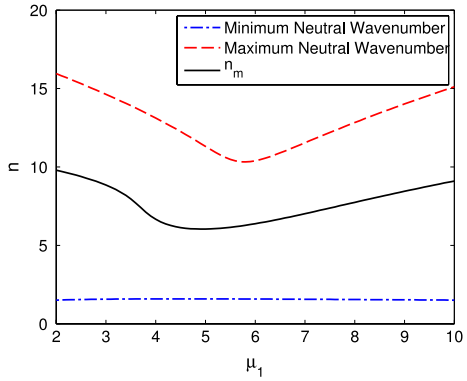


FIG. 9. Plots of the neutral wavenumbers and most dangerous wavenumber, $n_m$, versus the viscosity of the intermediate layer, $\mu_1$, for $R_0 = 20$, $R_1 = 22$, $\mu_i = 2$, $\mu_o = 10$, $Q = 10$, $T_0 = 1$, and $T_1 = 1$.

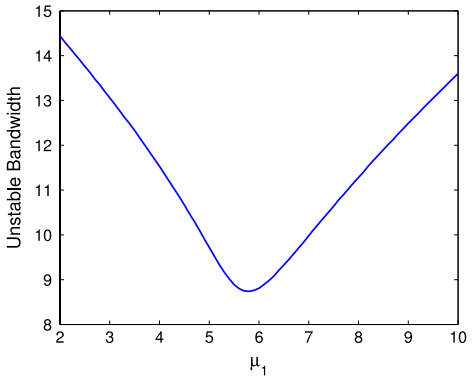


FIG. 10. A plot of the unstable bandwidth versus $\mu_1$ for $R_0 = 20$, $R_1 = 22$, $\mu_i = 2$, $\mu_o = 10$, $Q = 10$, $T_0 = 1$, and $T_1 = 1$.

### A. Validation of the upper bounds

First, we wish to validate the upper bound (47). In Figure 7, we plot the same dispersion curves as in Figure 4, labeled $\sigma_R^+$ and $\sigma_R^-$, but include the upper bound using several different values of $\lambda_1$ and $\lambda_2$. The parameter values are $R_0 = 20$, $R_1 = 30$, $\mu_i = 2$, $\mu_1 = 5$, $\mu_o = 10$, $Q = 10$, $T_0 = 1$, and $T_1 = 1$. The first upper bound we plot uses the values $\lambda_1 = \lambda_2 = 0$. This upper bound is given in equation (48). Recall that this is the worst upper bound. We can see that the upper bound is, in fact, an upper bound because it is greater than both $\sigma_R^+$ and $\sigma_R^-$ everywhere inside the unstable band. Recall that equation (47) consists of two terms, one corresponding to each interface. The discontinuity in the slope of the upper bound corresponds to the point where the term corresponding to the inner interface is equal to the term corresponding to the outer interface. We call this wavenumber $n^*$. When $n < n^*$, the term corresponding to one of the interfaces is larger, and when $n > n^*$, the term corresponding to the other interface is larger. Therefore, in essence, one region corresponds to wavenumbers where the inner interface is more unstable and the other region corresponds to wavenumbers where the outer interface is more unstable. Note that qualitatively, $\sigma_R^+$ has a similar shape to the upper bound. We also plotted the upper bound that comes from the values $\lambda_1 = \lambda_2 = 1/2$. This gives equal stabilization to the inner and outer interfaces. Note that this upper bound is an improvement over the previous upper bound, but has a similar shape. For the particular values of the parameters chosen here, the term corresponding to the inner interface is greater for $n < n^*$. Since this is the region where the growth rate is the largest, and, in fact, contains most of the unstable band, we optimize the upper bound by minimizing this term. Therefore, the maximal upper bound is given when $\lambda_1 = 1$ and $\lambda_2 = 0$. Clearly this upper bound is better than the previous two choices of the λ's for the most unstable wavenumbers.

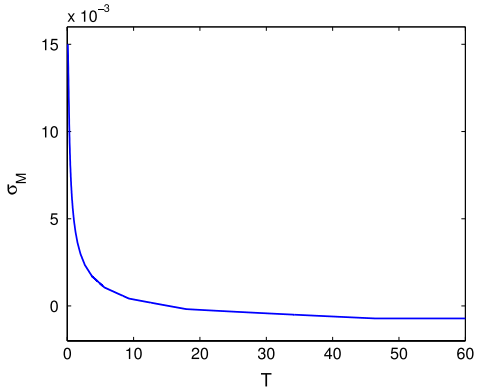


FIG. 11. A plot of the maximum growth rate versus interfacial tension for $R_0 = 20$, $R_1 = 30$, $\mu_i = 2$, $\mu_1 = 3$, $\mu_o = 10$, and $Q = 10$.

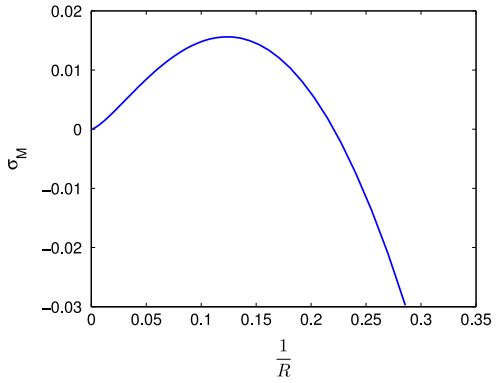


FIG. 12. A plot of the maximum growth rate versus the curvature of the interface for two-layer flow. The parameter values are $\mu_i = 2$, $\mu_o = 10$, $Q = 10$, and $T = 1$.

## B. The effect of the middle layer viscosity

Recall that we use $n_m$ to denote the wavenumber of the most dangerous wave and $\sigma_M$ to denote its growth rate. We now investigate the behavior of $\sigma_M$ under changes in the viscosity of the middle layer, $\mu_1$. We allow $\mu_1$ to vary between $\mu_i$ and $\mu_o$, which are 2 and 10, respectively. Here, we use the values $R_0 = 20$ and $R_1 = 22$ so that there will be sufficient interaction between the interfaces, and we use $Q = 10$. Figure 8 shows the results. The plot on the left uses the value $T_1 = 1$ and has curves corresponding to $T_0 = 1, 2, \ldots, 5$. The right plot uses $T_0 = 1$ and $T_1$ varies between 1 and 5. For each set of values $T_0$ and $T_1$, there is a value of $\mu_1$ within this range that minimizes $\sigma_M$. We would expect this because values near $\mu_i$ result in a large destabilizing jump in viscosity at the outer interface and values near $\mu_o$ result in a large destabilizing jump in viscosity at the inner interface. As $T_0$ increases in comparison to $T_1$, the value of $\mu_1$ that minimizes $\sigma_M$ increases because the stabilizing effect of interfacial tension on the inner interface counteracts the destabilizing effect of a larger viscous jump. Similarly, as $T_1$ increases in comparison to $T_0$, the value of $\mu_1$ that minimizes $\sigma_M$ decreases.

In Figure 9, we plot the values of the maximum neutral wavenumber, minimum neutral wavenumber, and $n_m$ versus $\mu_1$ for the values $T_0 = T_1 = 1$ (which corresponds to the solid line in each of the two plots in Figure 8). The unstable band consists of those wavenumbers between the maximum and minimum neutral waves. Note first that there is a value of $\mu_1$ that minimizes $n_m$. This value, seen as the minimum point of the middle curve in Figure 9, is relatively close to the value that minimizes $\sigma_M$. However, there is a different value of $\mu_1$ that minimizes the unstable bandwidth. To see this, we plot the unstable bandwidth versus $\mu_1$ in Figure 10.

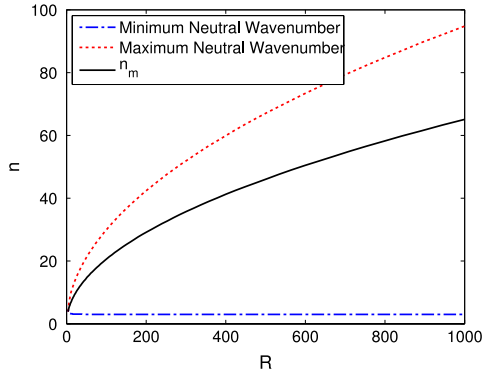


FIG. 13. Plots of the neutral wavenumbers and most dangerous wavenumber, $n_m$, versus the radius of the interface for two-layer flow. The parameter values are $\mu_i = 2$, $\mu_o = 10$, $Q = 10$, and $T = 1$.

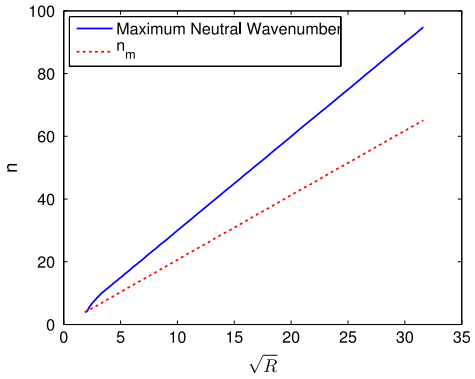


FIG. 14. Plots of the neutral wavenumbers and most dangerous wavenumber, $n_m$, versus $\sqrt{R}$. The parameter values are $\mu_i = 2$, $\mu_o = 10$, $Q = 10$, and $T = 1$.

### C. The effect of interfacial tension

Next, we investigate the effect of the interfacial tension on $\sigma_M$. We use the same interfacial tension at each interface and denote $T = T_0 = T_1$. We also use the values $R_0 = 20$, $R_1 = 30$, $\mu_i = 2$, $\mu_1 = 3$, $\mu_o = 10$, and $Q = 10$. Figure 11 shows the results. Note that the values that minimize the three layer upper bounds as given in (50) are $T_0 = 15.9155$ and $T_1 = 167.1127$. Therefore, we know from (51) and our choice of $\mu_1$ that when $T > 167.1127$, $\sigma_M < 0$. We see from Figure 11 that, in fact, $\sigma_M < 0$ for much smaller values of $T$. Also, $\sigma_M$ decreases much more rapidly for small values of $T$ and appears to approach a fixed value in the large $T$ limit. This agrees with our analysis of the two-layer case in Sec. II which shows that for large $T$, $n = 1$ is the most dangerous wavenumber and the value of the growth rate at $n = 1$ is independent of $T$.

### D. The effect of the curvature of the interfaces

We now investigate the stability of the system for different values of the curvature of the interfaces. To elucidate the results for three-layer flows, we begin by investigating the effect of curvature in two-layer radial flows. Recall the expression for the growth rate, (12). Also, recall that $n_m = \sqrt{QR(\mu_o - \mu_i)/(6\pi T) + 1/3}$. Therefore, as $R \to 0$, the wave corresponding to $n = 1$ is the most dangerous wave. The growth of this wave is given by $\sigma_M = -(Q\mu_i)/(\pi R^2(\mu_o + \mu_i))$. In the limit as $R \to 0$, $\sigma_M$ decreases without bound like $-1/R^2$. Therefore, the flow is stable as the curvature of the interface increases to infinity. To investigate the limit as $R \to \infty$, we use (12) with $n = n_m$. Since $n_m$ is proportional to $\sqrt{R}$, this expression goes to zero as $R \to \infty$ at the rate $R^{-\frac{3}{2}}$.

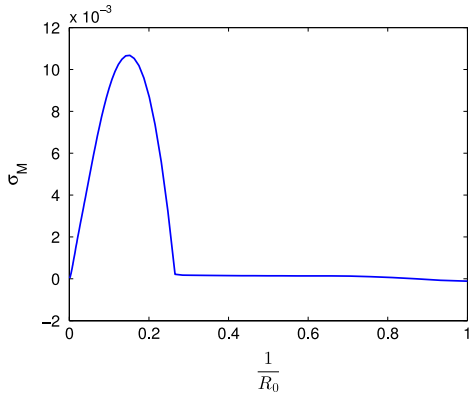


FIG. 15. A plot of the maximum growth rate versus the curvature of the inner interface for three-layer flow. The parameter values are $\mu_i = 2$, $\mu_1 = 6$, $\mu_o = 10$, $Q = 10$, $T_0 = 1$, and $T_1 = 1$.

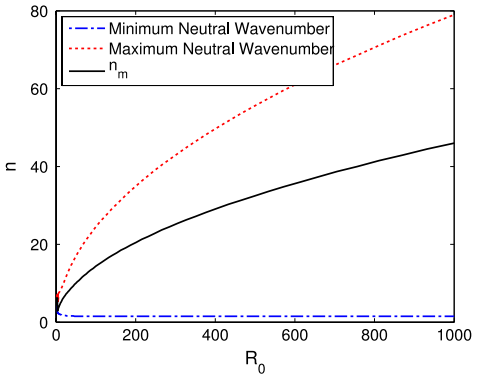


FIG. 16. Plots of the neutral wavenumbers and most dangerous wavenumber, $n_m$, versus the radius of the inner interface for three-layer flow. The parameter values are $\mu_i = 2$, $\mu_1 = 6$, $\mu_o = 10$, $Q = 10$, $T_0 = 1$, and $T_1 = 1$.

Therefore, $\sigma_M$ goes to zero as the curvature of the interface goes to zero. Physically, this results from the fact that the velocity of the interface goes to zero as $R \to \infty$. However, between these two limiting cases, the dependence of $\sigma_M$ on the curvature is not monotonic. Figure 12 shows $\sigma_M$ versus the curvature of the interface using the values $\mu_i = 2$, $\mu_o = 10$, $Q = 10$, and $T = 1$. We see that for large values of the curvature, the flow is stable. For small values of the curvature, the flow is unstable, but there is a finite value of curvature for which the flow is most unstable. We can also see the effect of the curvature on the unstable band and $n_m$. Figure 13 shows the values of the two neutral wavenumbers and $n_m$ versus $R$. As predicted by the expression for $n_m$ above, we see that as the interface moves outward and the curvature decreases, $n_m$ increases. Additionally, this is true for the maximum neutral wavenumber. This, combined with the fact that the minimum neutral wavenumber remains relatively fixed as $R$ increases, means that the decrease in curvature results in an increase in the unstable bandwidth. To investigate the exact rate of this increase in $n_m$ and the unstable bandwidth, we plot $n_m$ and maximum neutral wavenumber against $\sqrt{R}$ in Figure 14. Note that after an initial period, the growth of each of these values is linear. Therefore, when the interfaces are far from the origin, the unstable bandwidth and $n_m$ increase proportional to $\sqrt{R}$.

Next, we consider three-layer flow. We adjust the curvature of the inner interface while preserving the area of the fluid region between the interfaces. This is consistent with the basic solution whose stability we are investigating. Therefore, as the curvature of the inner interface decreases, so does the curvature of the outer interface. For Figures 15-17, we fix the area of the middle layer at $300\pi$. We use viscosity $\mu_1 = 6$ for the middle layer and interfacial tension $T_0 = T_1 = 1$. As the interfaces move farther away from the origin, there are several factors at play. First, the curvature of each interface is reduced. Also, the distance between the interfaces decreases, resulting in greater

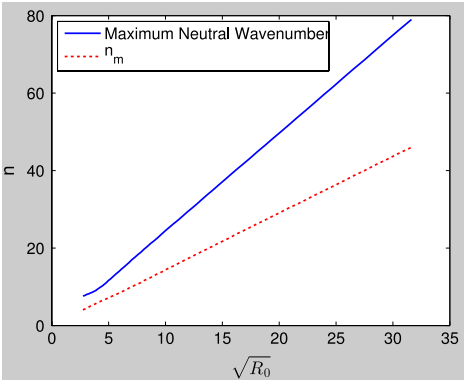


FIG. 17. A plot of the maximum neutral wavenumber and most dangerous wavenumber, $n_m$, versus $\sqrt{R_0}$. The parameter values are $\mu_i = 2$, $\mu_1 = 6$, $\mu_o = 10$, $Q = 10$, $T_0 = 1$, and $T_1 = 1$.

interaction between the interfaces. Figure 15 shows $\sigma_M$ versus the curvature of the inner interface. We see similar behavior to the two-layer case. As the curvature goes to zero, $\sigma_M$ approaches zero. There is some finite value of curvature for which the flow is most unstable. When the curvature is large, the flow is stable. The primary difference occurs for large values of curvature. Recall that in the two-layer case, $\sigma_M$ behaves like $-1/R^2$ in the large curvature limit. However, the curve in Figure 15 decays much more slowly for large values of curvature. This is due to the fact that the outer interface's curvature does not increase without bound. Therefore, it adds to the instability of the system as a whole. We also plot the neutral wavenumbers as well as $n_m$ versus the position of the inner interface. This plot is in Figure 16. As in two-layer flow, $n_m$ and the maximum neutral wavenumber increase with $R_0$, while the minimum neutral wavenumber remains relatively constant. Figure 17 shows that as $R_0$ becomes large, the unstable bandwidth and $n_m$ increase proportional to $\sqrt{R_0}$.

## VI. CONCLUSIONS

In this paper, we investigate the instability of multi-layer radial Hele-Shaw flows in which each layer of fluid has a constant viscosity. We obtain the following key results.

1. We provide a new formulation (see Sec. II) of the eigenvalue problem for two-layer radial Hele-Shaw flows. While previous formulations,[4,7,11] which only treat restricted cases, make use of the potential function, the current formulation does not. The advantage of this approach is that it can be extended to flows with variable viscosity fluids, which is the subject of a separate work in progress. Our formulation is able to reproduce the results previously found with the potential function approach.
2. We perform linear stability analysis of the multi-layer radial flows and obtain the associated eigenvalue problem. We perform analysis on this eigenvalue problem and obtain some results, some of which are summarized below.
3. We give an exact expression for the growth rate, $\sigma$, for three-layer flows (see Eq. (21)). Unlike two-layer radial flow (see Sec. II) and multi-layer rectilinear flow (see Ref. 23), $\sigma$ can be complex for three-layer radial flow. We also investigate (see Sec. III A) the thin-layer and thick-layer limit solutions. In the thick-layer limit, the two values of $\sigma$ are simply the two-layer growth rates of each interface. When the width of the middle layer is small, the unstable growth rate coincides with the two-layer growth rate that comes from the innermost and outermost fluid, with interfacial tension that is the sum of the interfacial tensions of the two interfaces.
4. Upper bounds are found for the real part of $\sigma$, denoted by $\sigma_R$, of the three-layer flow (see Eq. (47)). The upper bounds depend on two parameters, $\lambda_1$ and $\lambda_2$. When both are zero, we are able to find exact expressions for the wavenumbers that maximize the terms in the upper bound. These wavenumbers are the same as that of the most dangerous wave for each of the two individual interfaces in the two-layer setting. The use of these wavenumbers allows us to find an absolute upper bound on $\sigma_R$. Additionally, we give values of interfacial tension (see Eq. (50)) that minimize the upper bounds and can completely stabilize the flow. Their formulas coincide with the value of $T_o$ in the two-layer setting (see Sec. II).
5. We extend the three-layer upper bounds to flows with an arbitrary number of fluid layers (see Eq. (61)). Using this upper bound, we are able to show that the use of many thin layers of fluid with sufficiently small positive jumps in viscosity (in the direction of the basic velocity) at the interfaces improves upon the upper bound for the three-layer case. This indicates that it is likely that the addition of many layers of fluid with slowly varying viscosities is a good strategy for stabilization of the flow.
6. We reproduce several old results as limiting cases of the expression for $\sigma$. In particular, we obtain the growth rate of rectilinear Hele-Shaw flows found by Daripa.[23,24] We also show the result of Cardoso and Woods[11] by assuming that the inner interface is stable.
7. We numerically investigate the theoretical results for three-layer flows. We are able to validate the upper bounds and investigate the significance of the parameters $\lambda_1$ and $\lambda_2$. We also show that there are values of the middle layer viscosity that minimize both the instability of the most

dangerous wave and the unstable bandwidth. We show that the flow is completely stable for large enough values of interfacial tension.

8. We investigate the effect of curvature on the system. It is well known that rectilinear flow is always unstable when less viscous fluids are driving more viscous fluids.[23,24] This does not hold for radial flow in which the basic flow has curvature. We show that for large values of curvature, the flow is stable. The effect of curvature on the system is found to be non-monotonic, as there is a finite value of curvature that maximizes the instability of the flow. As the interfaces move far away from the origin and the curvature goes to zero, $\sigma_M$ goes to zero because the velocity of the interface goes to zero. This is consistent with two-layer flows as evident by Eq. (12).

## ACKNOWLEDGMENTS

The author, Prabir Daripa, would like to acknowledge the Grant No. NPRP 08-777-1-141 from the Qatar National Research Fund (a member of The Qatar Foundation). The author, Craig Gin, would like to acknowledge IGERT fellowship and graduate teaching assistantship from the Department of Mathematics. Additionally, the authors are grateful to the reviewers for their constructive criticism which has helped to improve the paper tremendously. The statements made herein are solely the responsibility of the authors.

[1] G. Homsy, "Viscous fingering in porous media," Annu. Rev. Fluid Mech. **19**, 271–311 (1987).
[2] P. Saffman, "Viscous fingering in Hele–Shaw cells," J. Fluid Mech. **173**, 73–94 (1986).
[3] P. Saffman and G. Taylor, "The penetration of a fluid into a porous medium or Hele-Shaw cell containing a more viscous liquid," Proc. R. Soc. London, Ser. A **245**, 312–329 (1958).
[4] L. Paterson, "Radial fingering in a Hele–Shaw cell," J. Fluid Mech. **113**, 513–529 (1981).
[5] J. Chen, "Growth of radial viscous fingers in a Hele–Shaw cell," J. Fluid Mech. **201**, 223–242 (1989).
[6] E. O. Dias and J. A. Miranda, "Determining the number of fingers in the lifting Hele-Shaw problem," Phys. Rev. E **88**, 043002 (2013).
[7] J. Miranda and M. Widom, "Radial fingering in a Hele-Shaw cell: A weakly nonlinear analysis," Phys. D **120**, 315–328 (1998).
[8] H. Power, "The evolution of radial fingers at the interface between 2 viscous liquids," Eng. Anal. Boundary Elem. **14**, 297–304 (1994).
[9] S. Rauseo, P. Barnes, Jr., and J. Maher, "Development of radial finger patterns," Phys. Rev. A **35**, 1245–1251 (1987).
[10] S. Sarkar and D. Jasnow, "Dynamics of immiscible radial viscous fingering — A numerical study," Pramana-J. Phys. **41**, 389–399 (1993).
[11] S. Cardoso and A. Woods, "The formation of drops through viscous instability," J. Fluid Mech. **289**, 351–378 (1995).
[12] T. Doscher and F. Wise, "Enhanced crude-oil recovery potential: Estimate," J. Pet. Technol. **28**, 575–585 (1976).
[13] *Enhanced Oil Recovery*, edited by F. Fayers (Elsevier, The Netherlands, 1981), p. 596.
[14] L. Lake, *Enhanced Oil Recovery* (Prentice Hall, Englewood Cliffs, NJ, 1989).
[15] W. Littman, *Polymer Flooding: Developments in Petroleum Science* (Elsevier, Amsterdam, 1998), p. 513.
[16] N. Mungan, "Improved waterflooding through mobility control," Can. J. Chem. Eng. **49**, 32–37 (1974).
[17] R. Needham and P. Doe, "Polymer flooding review," J. Pet. Technol. **12**, 1503–1507 (1987).
[18] G. Pope, "The application of fractional flow theory to enhanced oil-recovery," Soc. Pet. Eng. J. **20**, 191–205 (1980).
[19] G. Pope and R. Nelson, "A chemical flooding compositional simulator," Soc. Pet. Eng. J. **18**(5), 339–354 (1978).
[20] *Improved Oil Recovery by Surfactants and Polymer Flooding*, edited by D. Shah and R. Schecter (Academic Press, New York, NY, 1977), p. 513.
[21] K. Sorbie, *Polymer-Improved Oil Recovery* (CRC Press, Boca Raton, Florida, 1991), p. 513.
[22] A. Uzoigwe, F. Scanlon, and R. Jewett, "Improvement in polymer flooding: The programmed slug and the polymer-conserving agent," J. Pet. Technol. **26**, 33–41 (1974).
[23] P. Daripa, "Hydrodynamic stability of multi-layer Hele-Shaw flows," J. Stat. Mech.: Theory Exp. **2008**, P12005
[24] P. Daripa, "Studies on stability in three-layer Hele-Shaw flows," Phys. Fluids **20**, 112101 (2008).
[25] P. Daripa and X. Ding, "Universal stability properties for multi-layer Hele-Shaw flows and application to instability control," SIAM J. Appl. Math. **72**, 1667–1685 (2012).
[26] A. McBirney, *Ingenous Petrology* (Freeman, Cooper and Co., San Francisco, 1984).
[27] H. Darcy, *Les Fontaines Publiques de la Ville de Dijon* (Dalmont, Paris, 1856).